Journal of Materials Chemistry C

ROYAL SOCIETY OF CHEMISTRY

PAPER

The effect of the terminal linking atom on the appearance of twist-bend nematic and smectic phases

Ewan Cruickshank, [ID] †*[a] Grant J. Strachan, [ID] [ab] Magdalena M. Majewska, [ID] [b] Damian Pociecha, [ID] [b] Ewa Gorecka, [ID] [b] John M. D. Storey[a] and Corrie T. Imrie [ID] ‡[a]

The synthesis and characterization of five new members of both the CB6O·O*m* (6O defining the spacer as hexyloxy) and CBO5O·*m* (O5O defining the spacer as oxypentyloxy) series are reported which possess extended terminal alkyl chains. Two new series of dimers are also reported in which the linking group between the terminal alkyl chain and mesogenic unit is varied, namely the CBO5O·O*m* and CBO5O·S*m* series. All four series exhibit both the twist-bend nematic phase (N$_{TB}$) as well as a rarely reported twist-bend smectic C phase (SmC$_{TB-SH}$). X-ray diffraction measurements showed that the SmC$_{TB-SH}$ phase had a partially interdigitated bilayer packing arrangement in agreement with previous literature reports. The phase behaviour between these four series and the previously reported CB6O·*m* and CB6O·S*m* series are compared. The N$_{TB}$ phase is observed when the terminal alkyl chains are short whereas when the terminal alkyl chains are long there is a predisposition towards more smectic-like behaviour such as the SmC$_{TB-SH}$ phase. The dimers which contain an oxygen link in the terminal chain have higher values of T_{NTBN} than those with a sulfur or methylene link. Additionally, the dimers with an 6O spacer, in general, had slightly higher values than those with O5O spacers. Interestingly, the SmC$_{TB-SH}$ phase did follow the same trend with regards to the effect of the terminal linking group but the reverse trend with regards to the spacer.

Introduction

The twist-bend nematic (N$_{TB}$) phase is a rare example of spontaneous chirality generated by achiral molecules and has attracted a huge amount of research interest since its experimental discovery in 2011.[1] It is a nematic phase, so the molecules have a preferred orientation, known as the director, however the director in this phase rotates to form a heliconical structure.[2,3] The director is tilted with respect to the helical axis, and the pitch length in the N$_{TB}$ phase is typically only 10s of nm; far shorter than those seen for inherently chiral phases such the chiral nematic phase.[4,5] The typical N$_{TB}$ pitch corresponds to only around 3 or 4 molecular lengths. There has been a great deal of effort made to identify the molecular features that promote the N$_{TB}$ phase, and a key requirement is a bent

molecular shape.[6,7] This fits with the theoretical predictions of twist-bend behaviour made independently by Meyer and Dozov.[8,9] The majority of reported twist-bend nematogens have been dimeric molecules, in which two mesogenic units are linked by an odd-membered flexible spacer,[10–23] but a range of other structures have also been reported such as trimers,[24–27] tetramers,[28,29] higher oligomers,[30–32] bent-core mesogens,[33,34] hydrogen-bonded systems[35–38] and chiral mesogens.[39–43] There has recently been an even-membered dimer reported which exhibited the N$_{TB}$ phase.[44]

In his 2001 work, Dozov not only predicted the existence of the N$_{TB}$ phase but also that there could be twist-bend smectic phases (SmC$_{TB}$) with a similar degree of symmetry breaking.[9] This proved challenging to investigate experimentally, as it was assumed any SmC$_{TB}$ phases would have to follow the N$_{TB}$ phase and most compounds exhibiting the N$_{TB}$ phase would vitrify or crystallise on cooling.[37] The first experimental observation of a SmC$_{TB}$ phase was reported in 2018 in a series of asymmetric dimers which were part of the CB6OIBeO*n* series.[45] The molecules contained one cyanobiphenyl mesogenic group, a second mesogenic group consisting of three aromatic rings connected by an ester and an imine group, a hexyloxy flexible spacer and a

[a] Department of Chemistry, University of Aberdeen, Old Aberdeen, AB24 3UE, UK.
E-mail: e.cruickshank2@rgu.ac.uk
[b] Faculty of Chemistry, University of Warsaw, Pasteura 1, 02-093 Warsaw, Poland
† Present Address: School of Pharmacy, Applied Sciences and Public Health, Robert Gordon University, Aberdeen, AB10 7GJ, UK.
‡ Deceased 14th January 2025.

Paper

terminal alkyloxy chain. Importantly, this discovery revealed that the formation of the SmC$_{TB}$ phase did not require a preceding N$_{TB}$ phase at higher temperatures, despite the earlier predictions. This first twist-bend smectic phase was called SmC$_{TB-\alpha}$, and its helical nature was confirmed by resonant soft X-ray scattering (RSoXS) measurements.[46] Non-resonant X-ray diffraction measurements showed the phase has a monolayer structure, with a periodicity comparable to the molecular length. The helical pitch was comparable to that of the N$_{TB}$ phase, at around 12–15 nm. The SmC$_{TB-\alpha}$ phase has also been observed in other dimers with a similar molecular structure.[47] More recently, new variants of the SmC$_{TB}$ phase have been identified. These phases, known as the SmC$_{TB-SH}$ and SmC$_{TB-DH}$ phases,[48,49] have a structure which can be described as a distorted clock where the azimuthal angle between the long molecular axis in adjacent smectic layers is different than 90°. This 'distorted clock' structure makes the SmC$_{TB-SH}$ phase optically biaxial. In RSoXS studies, the SmC$_{TB-SH}$ phase showed a resonance peak corresponding to 4 molecular layers, while non-resonant X-ray diffraction revealed a bilayer structure. The SmC$_{TB-DH}$ phase, while also adopting a four-layer helix with distorted clock structure, also has an additional shift in azimuthal angle between consecutive layers which results in a longer helical modulation being superimposed on the basic 4-layer helix structure. This additional helix makes the phase optically uniaxial.[50] The unwinding of the secondary helix in the SmC$_{TB-DH}$ phase on approaching the SmC$_{TB-SH}$ phase gave the first observation of selective reflection of light in an achiral mesogen.[48] These apolar twist-bend smectic phases have been found in a range of non-symmetric bent dimers;[51–54] however, the structure–property relationships of these materials are still poorly understood. Understanding these relationships is key not only in the design of new compounds which exhibit the twist-bend smectic C phases but also to potentially discover new phases in this realm.

Here we investigate the effect of the linking group between the mesogenic unit and the terminal chain on the formation of the twist-bend nematic and single-helix twist-bend smectic C phases. In this work, we have started from a dimeric structure consisting of a cyanobiphenyl mesogenic group, an oxypentyloxy spacer (also referred to later as O5O with 5 being the number of carbons in the spacer), and a benzylideneaniline

mesogenic unit with an alkyl terminal chain. This structure is similar to the CB6O·m series[48,53] (which has an hexyloxy spacer hence referred to as 6O with 6 being the number of carbons in the spacer) which was the first series reported to form the SmC$_{TB-SH}$ phase, but with two ether links in the central spacer. Changing the linking groups in the central spacer of a dimer will change the degree of molecular bend, and as this has been shown to strongly influence the formation of the N$_{TB}$ phase, it may be expected to also have an important role in the formation of twist bend smectic phases. We report three series of liquid crystal dimers, with oxypentyloxy spacers, the CBO5O·m series, Fig. 1(a), the CBO5O·Om series, Fig. 1(b), and the CBO5O·Sm series, Fig. 1(c), changing the nature of the terminal linking group. We also report on new members of the CB6O·Om series, Fig. 1(d), which is analogous to the CB6O·m series[53] but with an oxygen terminal linking group. In addition to considering the influence of the central spacer through comparison to the analogous CB6O·m series, this allows us to investigate the role of the terminal linking group in more depth. The transition temperatures of the CBO5O·m and CB6O·Om series for m = 1 to 10 have been reported previously.[37,53,55] However, as extending the terminal chain length is expected to promote additional smectic polymorphism, the aim is to establish if the twist-bend smectic C phases may also be observed despite the more linear structure.

Experimental

The synthetic route used to prepare the CBO5O·m series is shown in Scheme 1, the CBO5O·Om series in Scheme 2, the CBO5O·Sm series in Scheme 3 and CB6O·Om series in Scheme 4 in the SI along with a detailed description of the preparation of all members of these series, including the structural characterisation data for all intermediates and final products.

Optical studies

Phase characterisation was performed by polarised light microscopy, using an Olympus BH2 polarising light microscope equipped with a Linkam TMS 92 hot stage. The untreated glass microscope slides used were 0.17 mm thick. The cells treated for planar alignment were purchased from INSTEC, were 2.9–3.5 µm thick and possessed transparent ITO electrodes.
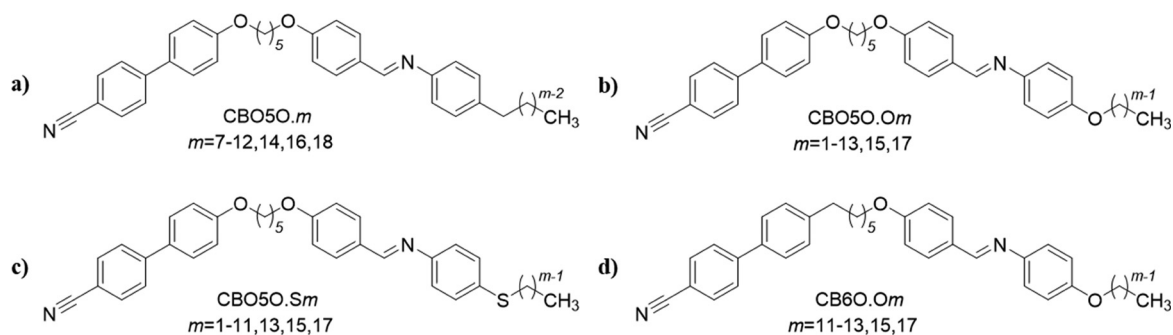

Fig. 1 Molecular structures of the (a) CBO5O·m, (b) CBO5O·Om, (c) CBO5O·Sm and (d) CB6O·Om series.

Differential scanning calorimetry

The phase behaviour of the materials was studied by differential scanning calorimetry performed using a Mettler Toledo DSC1 or DSC3 differential scanning calorimeter equipped with TSO 801RO sample robots and calibrated using indium and zinc standards. Heating and cooling rates were 10 °C min^{-1}, with a 3-min isotherm between either heating or cooling, and all samples were measured under a nitrogen atmosphere. Transition temperatures and associated enthalpy changes were extracted from the heating traces unless otherwise noted.

Molecular modelling

The geometric parameters of all three series of dimers were obtained using quantum mechanical DFT calculations with Gaussian09 software.[56] Optimisation of the molecular structures was carried out at the B3LYP/6-311G(d,p) or B3LYP/6-31G(d) level of theory. Comparison of the results of optimisation of the methylene- and ether-linked dimers at the B3LYP/6-311G(d,p) and the 6-31G(d) levels showed no discernible difference in the geometries found, and so optimisation of the methylene- and ether-linked dimers was carried out at the B3LYP/6-31G(d) level. Visualisations of electronic surfaces and ball-and-stick models were generated from the optimised geometries using the Gauss-View 5 software, and visualisations of the space-filling models were produced post-optimisation using the QuteMol package.[57]

X-Ray diffraction measurements

The X-ray diffraction measurements were obtained with a Bruker D8 GADDS system (CuKα line, Goebel mirror, point beam collimator, Vantec2000 area detector). Samples were prepared as droplets on a heated surface. The temperature dependence of the layer thickness was determined from the small-angle X-ray diffraction experiments obtained with a Bruker Nanostar system using CuKα radiation and patterns were collected with a Vantec2000 area detector.

Birefringence measurements

Optical birefringence was measured with a setup based on a photoelastic modulator (PEM-90, Hinds) working at a modulation frequency f = 50 kHz; as a light source, a halogen lamp (Hamamatsu LC8) was used equipped with narrow bandpass filter (532 nm). The signal from a photodiode (FLC Electronics PIN-20) was deconvoluted with a lock-in amplifier (EG&G 7265) into $1f$ and $2f$ components to yield a retardation induced by the sample. Knowing the sample thickness, the retardation was recalculated into optical birefringence. Samples were prepared in 1.6-μm-thick cells with planar anchoring. The alignment quality was checked prior to measurement by inspection under the polarised light optical microscope.

Results

The transitional properties for the CBO5O·m series are listed in Table S8 with the entropy values associated with the liquid crystal transitions being reported after scaling their values by the gas constant, R. The phase behaviour for m = 1–10 has been reported previously.[53–55] The original reports for some members
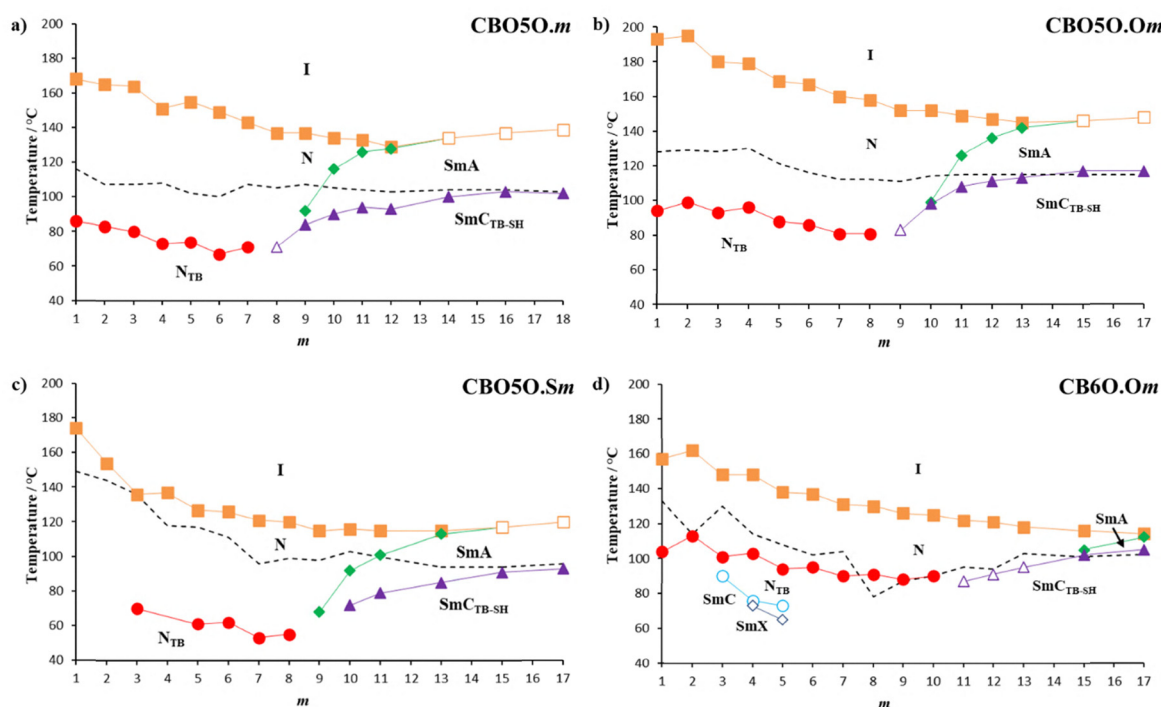

Fig. 2 Dependence of the transition temperatures on the length of the terminal alkyl chain, m, for the (a) CBO5O·m (b) CBO5O·Om (c) CBO5O·Sm and (d) CB6O·Om series represented by filled squares for T_{NI}, filled circles for T_{NTBN}, open squares for T_{SmAI}, open circles for T_{SmCNTB}, open diamonds for T_{SmXSmC}, filled diamonds for T_{SmAN}, open triangles for $T_{SmCTB-SHN}$, filled triangles for $T_{SmCTB-SHSmA}$, and the dotted line indicates the melting points.

of the series preceded the discovery of the N$_{TB}$ and SmC$_{TB}$ phases and where relevant the phases have been reassigned. The dependence of the transition temperatures on the length of the terminal alkyl chain, m, for the CBO5O·m series is shown in Fig. 2(a).[53,55] The new homologues synthesised, $m \geq 11$, exhibited either the conventional nematic phase or the smectic A phase on cooling from the isotropic phase. The values of $\Delta S_{NI}/R$ are consistent with this phase assignment and the values of $\Delta S_{SmAI}/R$ are clearly larger than those of $\Delta S_{NI}/R$ due to the increase in the order parameter. All these new homologues also exhibited the SmC$_{TB-SH}$ phase on cooling prior to crystallisation.

The transitional properties for the CBO5O·Om series are listed in Table S9 and the dependence of the transition temperatures on the length of the terminal alkoxy chain, m, for the CBO5O·Om series is shown in Fig. 2(b). The homologues with an alkoxy chain with $m \leq 13$ showed a conventional enantiotropic nematic phase, N. Succeeding the nematic phase when $m \leq 8$ is the N$_{TB}$ phase, when $m = 9$ the N$_{TB}$ was replaced by the SmC$_{TB-SH}$ phase, and when $m = 10$–13 the phase is followed by the conventional SmA phase. At the longest chain lengths, $m = 15$ and 17, a direct transition between the isotropic liquid and smectic A phase is seen. In all the homologues which contain the SmA phase, the SmC$_{TB-SH}$ phase is also observed at lower temperatures.

The transitional properties for the CBO5O·Sm series are listed in Table S10 and the dependence of the transition temperatures on the length of the terminal alkylthio chain, m, for the CBO5O·Sm series is shown in Fig. 2(c). For $m \leq 13$ a conventional nematic phase, was observed, and the values of

$\Delta S_{NI}/R$ are consistent with this assignment. The N$_{TB}$ phase was preceded by the nematic phase in pure samples of the CBO5O·Sm series for $m = 5$–8. For $m \leq 4$, the twist-bend nematic phase was not observed, presumably due to crystallisation precluding its appearance. The N$_{TB}$ phase was extinguished and instead the SmA phase was observed when $m \geq 9$, with direct transitions between the SmA phase and isotropic liquid when $m = 15$ and 17. Underlying the SmA phase when $m \geq 10$ is the SmC$_{TB-SH}$ phase.

The transitional properties for the CB6O·Om series, $m = 1$ to 10, have been reported in the literature,[37] while those of the new members are listed in Table S11 and the dependence of the transition temperatures on the length of the terminal alkoxy chain, m, for the CB6O·Om series is shown in Fig. 2(d).[37] The new homologues synthesised here show a clear difference in mesogenic behaviour compared to the dimers with a shorter terminal chain. All the new homologues, $m \geq 11$, exhibit a conventional nematic phase on cooling the isotropic liquid phase and for all these homologues the lowest temperature mesophase is the SmC$_{TB-SH}$ phase. When $m = 11$, the N$_{TB}$ phase is observed prior to the observation of the SmC$_{TB-SH}$ phase while for $m = 15$ and 17 the nematic phase is succeeded by the SmA phase prior to the observation of the SmC$_{TB-SH}$ phase.

The phase behaviour in all four mesogenic series was initially assigned on the basis of observations made using polarised optical microscopy. The nematic phase was assigned based on the observation of a characteristic schlieren texture containing both two- and four-point singularities which flashed when subjected to mechanical stress, Fig. 3(a)–(d).
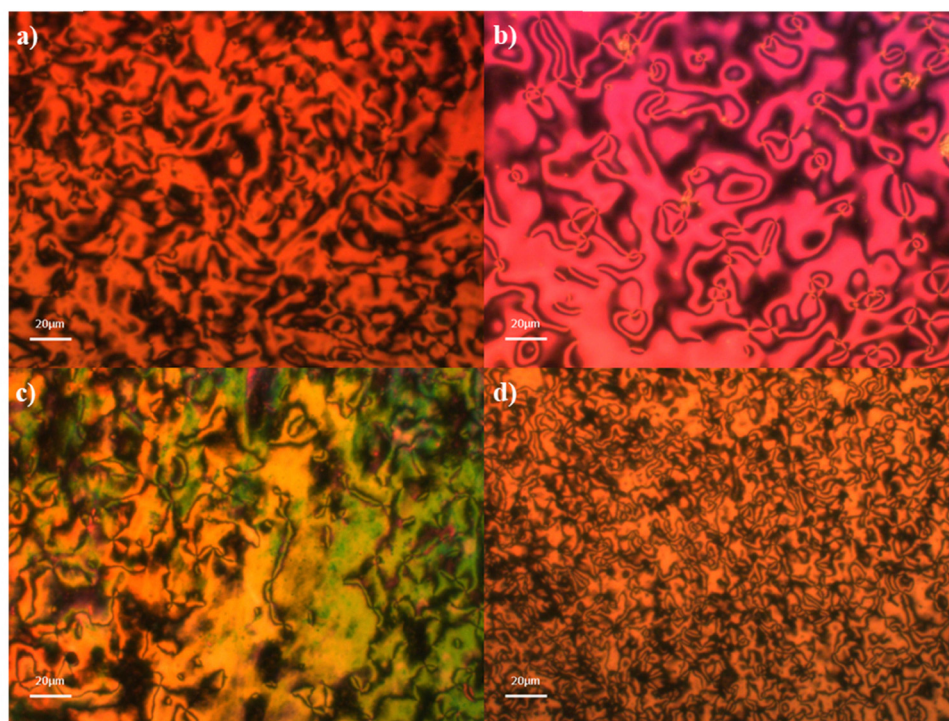

Fig. 3 Textures of the nematic phase: (a) schlieren texture ($T = 132$ °C) for CBO5O·10, (b) schlieren texture ($T = 152$ °C) for CBO5O·O10, (c) schlieren texture of ($T = 170$ °C) for CBO5O·S1 and (d) schlieren texture ($T = 115$ °C) for CB6O·O15.

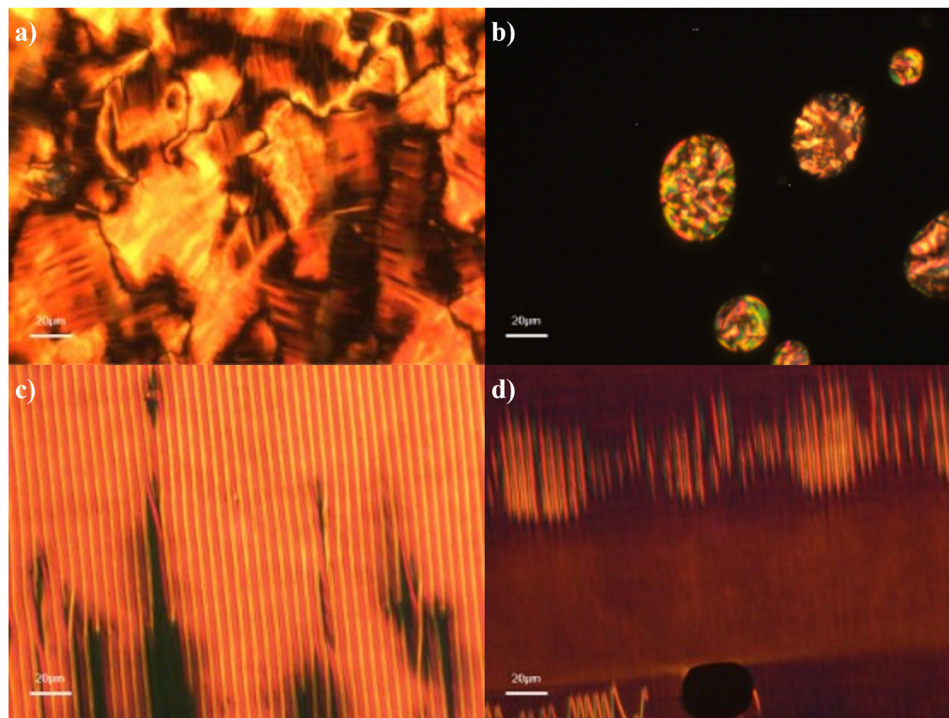**Fig. 4** Textures of the twist–bend nematic phase: (a) blocky schlieren texture (T = 73 °C) for CBO5O·O7, (b) blocky schlieren texture seen in isolated droplets (T = 54 °C) for CBO5O·S6, (c) striped texture in a planar aligned cell (T = 73 °C) for CBO5O·O7 and (d) striped texture in a planar aligned cell (T = 53 °C) for CBO5O·S8.

When the nematic phase was cooled, a cessation of the director fluctuations associated with the conventional nematic phase was observed and a blocky schlieren texture was instead observed, Fig. 4(a) and (b). In planar aligned cells a striped texture was observed characteristic of the twist-bend nematic phase, Fig. 4(c) and (d).

Due to the monotropic nature of the twist-bend nematic phase shown by some members of the CBO5O·Om series, the homologues with short terminal chains tended to only show the phase in isolated droplets. Thus, CBO5O·O3 was used as a representative example in a miscibility study with CB7CB to confirm the N$_{TB}$ assignment, see Fig. S1. Complete miscibility between the two compounds was observed over the whole composition range,

indicating the same phase behaviour. The higher temperature mesophase was a conventional nematic phase, Fig. 5(a) and on cooling, the twist-bend nematic phase formed, Fig. 5(b). The measured value of T_{NTBN} for CBO5O·O3 fits perfectly on the trend-line drawn for the mixtures, confirming the phase assignment.

For the CBO5O·Sm series, when $m \leq 4$, the N$_{TB}$ phase was not observed due to the early onset of crystallisation. In order to therefore estimate a virtual transition temperature for T_{NTBN}, a phase diagram was constructed with binary mixtures of CBO5O·S3 and CB7CB, see Fig. S2. Complete miscibility between the two compounds was observed over the whole composition range, indicating the same phase behaviour. The higher temperature mesophase for all mixtures studied was a
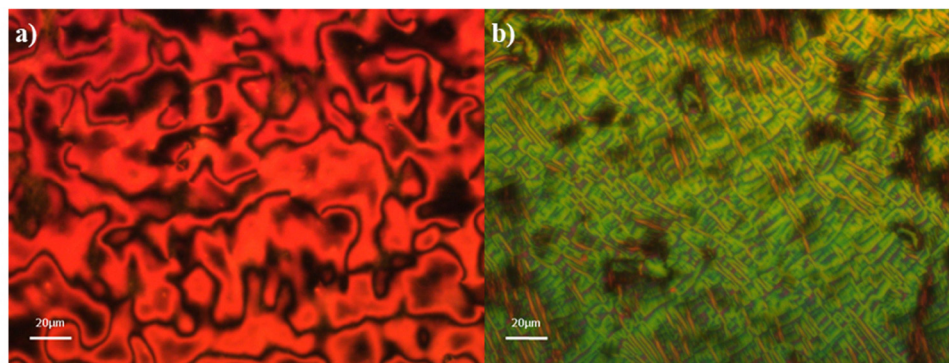

Fig. 5 Textures observed for the 40 : 60 mol% mixture of CB7CB : CBO5O·O3: (a) schlieren texture of the nematic phase (T = 135 °C) and (b) rope-like texture of the twist–bend nematic phase (T = 80 °C).

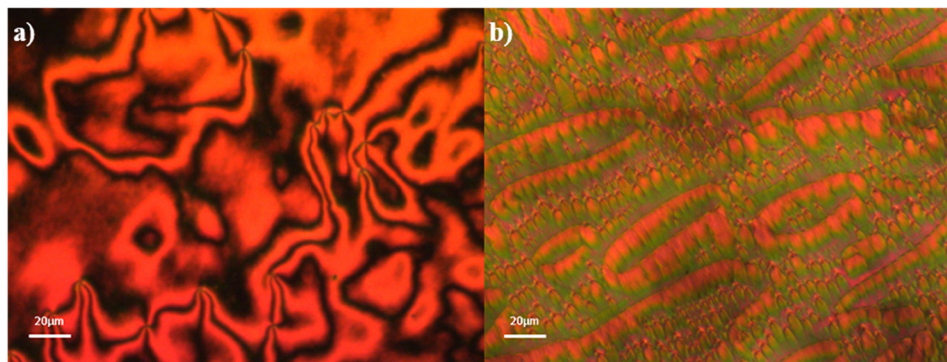**Fig. 6** Textures observed for the 40 : 60 mol% mixture of CB7CB : CBO5O·S3: (a) schlieren texture of the nematic phase (T = 117 °C) and (b) parabolic texture of the twist–bend nematic phase (T = 81 °C).

conventional nematic phase, see Fig. 6(a). On cooling the nematic phase, characteristic textures of the twist-bend nematic phase were observed, see Fig. 6(b). The T_{NI} trendline increases with the concentration of CBO5O·S3 and displayed a small downwards curvature, suggesting that the intermolecular energy parameter between the unlike species is smaller than the geometric mean of the interaction parameters between the like species.[58] The T_{NTBN} trendline also varied in essentially a linear sense but decreased with increasing concentrations of CBO5O·S3. The virtual transition temperature estimated for T_{NTBN} was 69 °C but it should be noted that this represents a rather extended extrapolation and was well below the bulk crystallisation temperature of the pure sample.

The SmA phase was assigned based on the observation of a characteristic focal conic fan texture which co-existed with regions of extinction, suggesting that the phase was optically uniaxial, Fig. 7(a)–(d).

The SmC$_{TB-SH}$ phase was assigned based on the observation of a focal conic fan texture which could be sheared to give regions containing a weakly birefringent schlieren texture consisting of mainly four-point brush defects, Fig. 8(a). The phase also was observed to contain areas which consisted of a pseudo-schlieren texture with moving stripes of different birefringence, Fig. 8(b)–(e). These striped textures appeared similar to those we have reported for the SmC$_{TB-SH}$ phase previously and seem to be characteristic of the phase. The focal conic fans initially
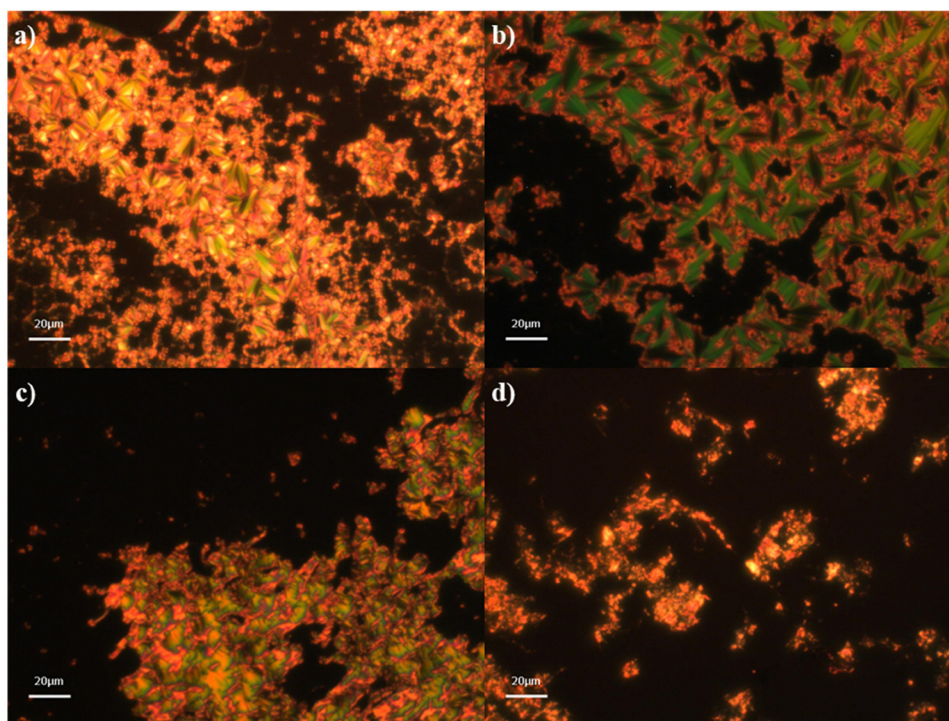

Fig. 7 Textures of the smectic A phase: (a) focal conic fan texture with homeotropic regions (T = 136 °C) for CBO5O·16, (b) focal conic fan texture with homeotropic regions (T = 147 °C) for CBO5O·O17, (c) focal conic fan texture with homeotropic regions (T = 85 °C) for CBO5O·S11 and (d) focal conic fan texture with homeotropic regions (T = 108 °C) for CB6O·O17.
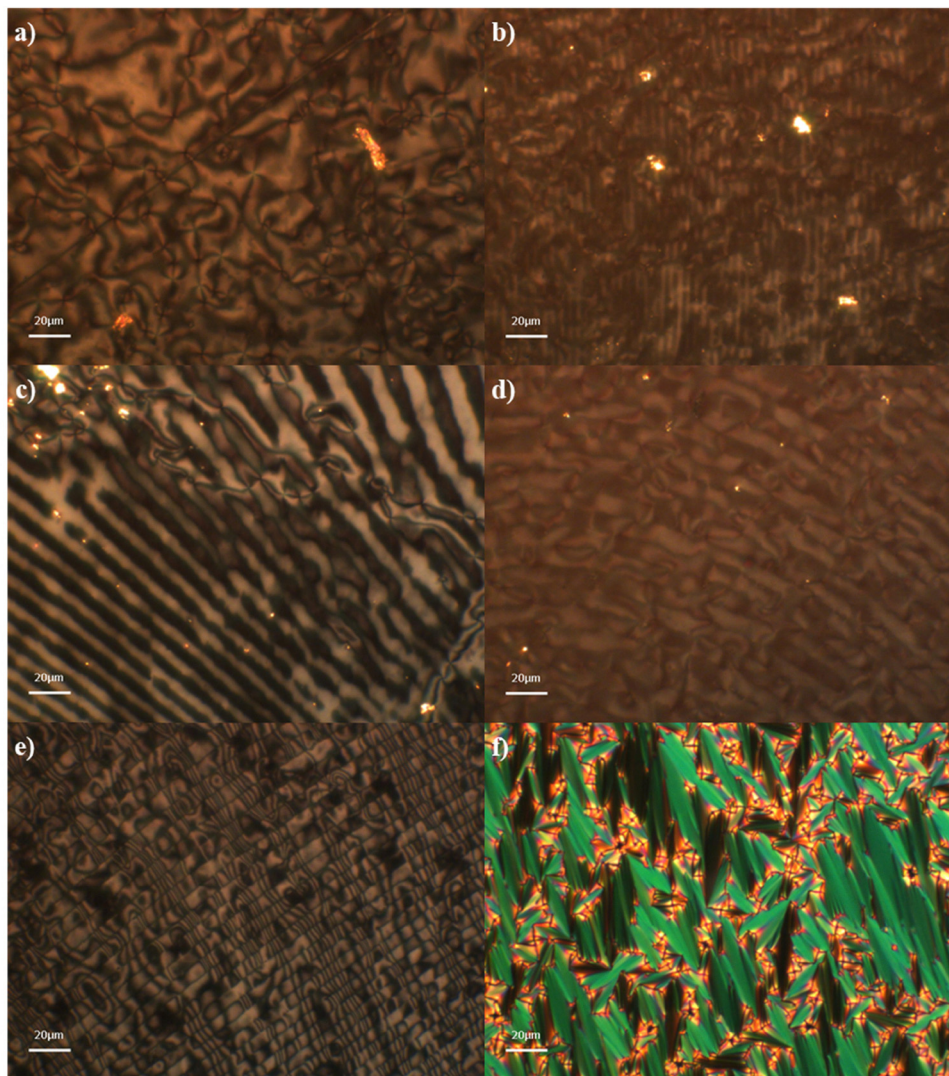
Fig. 8   Textures of the smectic C$_{TB-SH}$ phase: (a) weakly birefringent schlieren texture (T = 100 °C) for CBO5O·14, (b) pseudo-schlieren texture with moving stripes of opposing birefringence (T = 101 °C) for CBO5O·16, (c) pseudo-schlieren texture with moving stripes of opposing birefringence (T = 113 °C) for CBO5O·13, (d) pseudo-schlieren texture with moving stripes of opposing birefringence (T = 85 °C) for CBO5O·S13, (e) pseudo-schlieren texture with moving stripes of opposing birefringence (T = 90 °C) for CB6O·O15 and (f) focal conic fan texture in a planar aligned cell (T = 85 °C) for CBO5O·S15.

appeared smooth, Fig. 8(f) and when the sample was further cooled, lines developed across the fans, due to the onset of crystallisation.

X-ray diffraction studies were performed to confirm the phase sequences in selected members of each series, and this data is given in Fig. 9 and Fig. S3–S10. The observed trends were consistent across all materials studied.

As a representative example, the temperature dependence of the layer spacing in CBO5O·10 measured using small angle X-ray diffraction is given in Fig. 9. The transition from the N to the SmA phase was accompanied by narrowing of the width of the low angle X-ray diffraction signal, confirming the increase of the positional correlations in the nematic phase on approaching the transition to a lamellar phase. The layer spacing continuously increased on cooling through the SmA phase, indicating a negative thermal expansion, which is typical for SmA phases. On entering the SmC$_{TB-SH}$ phase, the layer spacing is ~72 Å, corresponding to just under twice the molecular length indicating a partially interdigitated bilayer packing arrangement. This was also observed for all the other dimers exhibiting the phase which were measured using X-ray diffraction, Fig. S3–S10, and is standard for the SmC$_{TB-SH}$ phase as we have reported previously.[48,49,51,52] Interdigitated packing in these dimers is driven by the antiparallel association of the cyanobiphenyl units, and due to the enhanced molecular inhomogeneity driven by the elongated terminal alkyl chains. The liquid-like nature of both the SmA and SmC$_{TB-SH}$ phases is confirmed by X-ray diffraction, as the wide-angle signal remained diffuse on cooling through both phases. (Fig. 9 inset).

The optical birefringence, Δn, increases quickly in the nematic phase following a critical dependence for both CB6O·O11 and CB6O·O13, Fig. 10. The measured birefringence starts
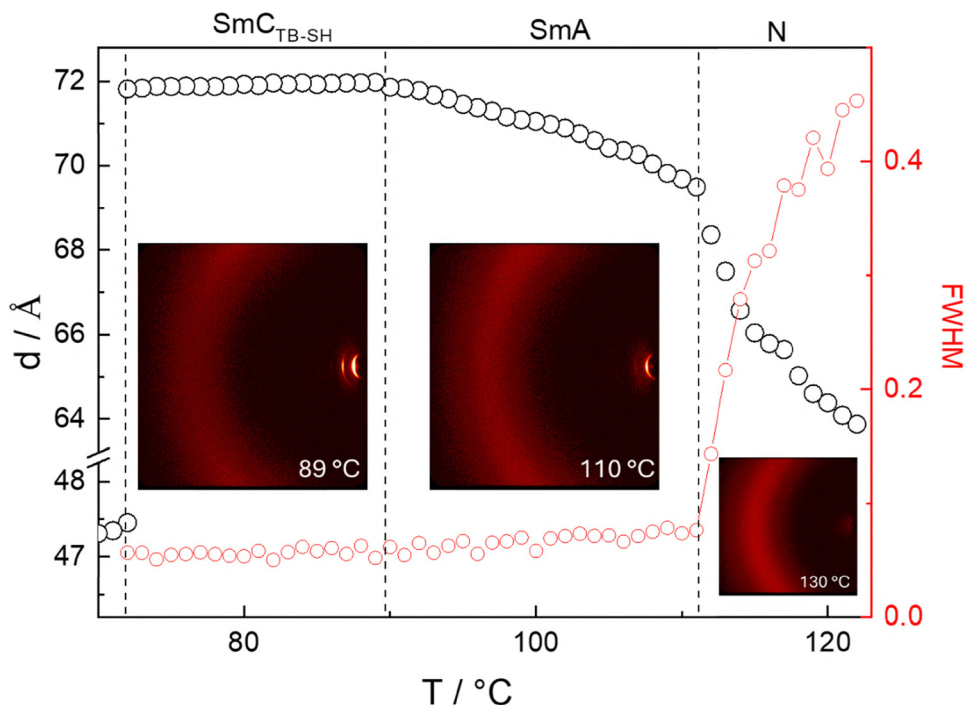
Fig. 9 The dependence of the layer spacing (d) on temperature for CBO5O·10 measured on cooling (black circles) and the dependence of the full width at half maximum on temperature (red circles). (Inset) The 2D X-ray diffraction patterns of CBO5O·10 for the SmC_{TB-SH}, SmA and N phases.
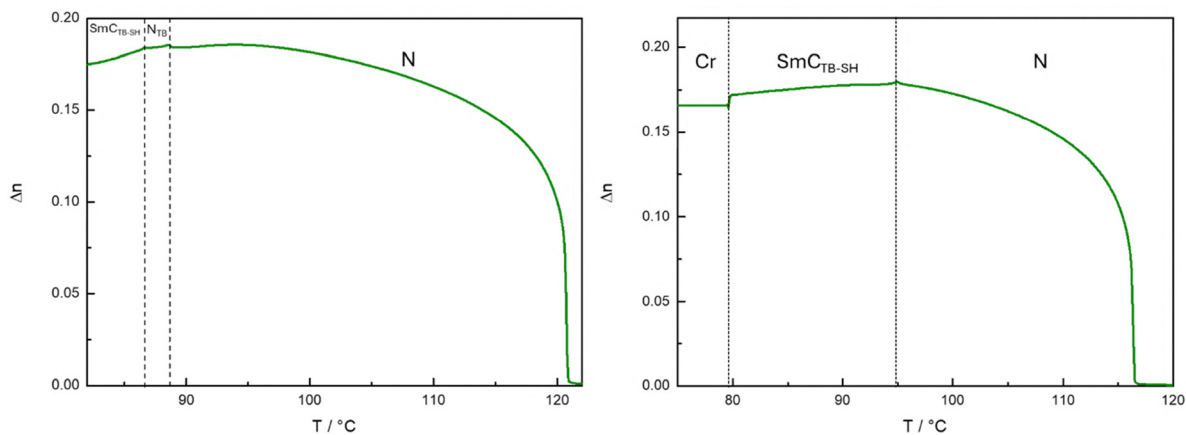

Fig. 10 The temperature dependence of the optical birefringence of (left) CB6O·O11 and (right) CB6O·O13 for green light (λ = 532 nm) in a 1.6 µm planar cell.

to depart from this critical dependence in CB6O·O11 on cooling the N phase towards the transition to the N_{TB} phase and this has been attributed to the formation of instantaneous local heliconical states. There is a small jump in Δn before the values decrease further due to the tilt of the molecules from the helical axis. There is another small step in Δn at the transition to the SmC_{TB-SH} phase presumably due to the increase in orientational ordering due to the layered nature of the smectic phase. The gradual decrease in Δn persists after the transition due to the molecules continuing to be tilted in the phase. For CB6O·O13 the N_{TB} phase is not observed and instead the SmC_{TB-SH} is directly seen after the conventional nematic phase. There is

again a small step increase at the transition before Δn decreases as the molecules tilt within the layered structure of the SmC_{TB-SH} phase, Fig. 10.

Discussion

The dependence of T_{NI} on the length of the terminal chain up to a total terminal chain length of 10 for the CBO5O·m,[53–55] CBO5O·Om and CBO5O·Sm series is shown in Fig. 11(a). These clearing temperatures are also compared against the CB6O·m, CB6O·Om and CB6O·Sm series which have been previously
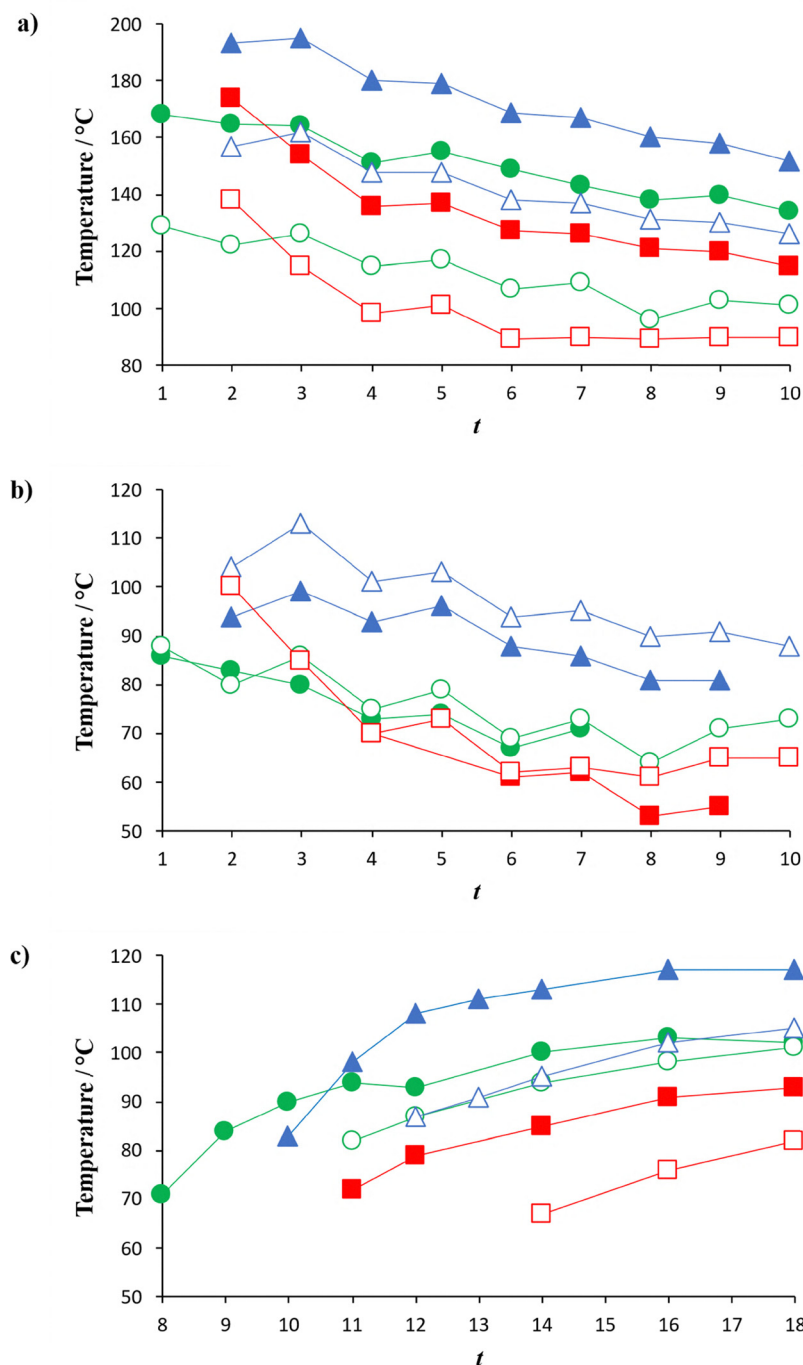
Fig. 11 Dependence of (a) T_{NI}, (b) T_{NTBN} and (c) $T_{SmCTB-SH-X}$, with total terminal chain length, t, for the CBO5O·m[53–55] series denoted by filled circles, the CBO5O·Om series denoted by filled triangles, the CBO5O·Sm series denoted by filled squares, the CB6O·m[48,53] series denoted by empty circles, the CB6O·Om[37] series denoted by empty triangles and the CB6O·Sm[52] series denoted by empty squares.

reported in the literature.[37,48,52,53] Homologues which have the same total terminal chain length, t, are compared such that $t = m + 1$ for the CBO5O·Om, CBO5O·Sm, CB6O·Om and CB6O·Sm series, whereas $t = m$ for the CBO5O·m and CB6O·m series. All six series showed fairly similar behaviour as the length of the terminal chain increased with T_{NI} generally decreasing. This may be attributed to the dilution of the interactions between

the mesogenic units on increasing the volume fraction of alkyl chains. The values of T_{NI} also tended to alternate based on the parity of the terminal chain and this is known as the odd–even effect.[59] When the total terminal chain length is odd, T_{NI} is expected to be higher or show a more gradual decrease in value than those of the adjacent even membered homologues. On changing the parity of the chain there is an enhanced change in
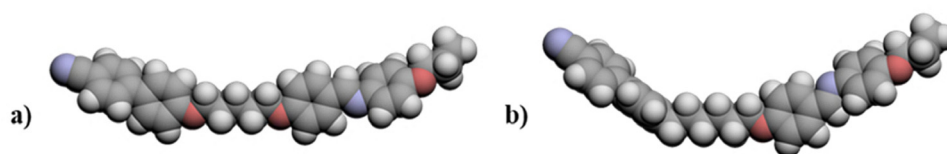
Fig. 12 A comparison of the molecular shapes of (a) CBO5O·O3 and (b) CB6O·O3.

the shape anisotropy when the chain is increased from being even-membered to odd-membered.

The oxygen-linked CBO5O·Om series showed the highest values of T_{NI} for all members of the series and in general dimers with an O5O spacer showed higher values than the comparable dimers with a 6O spacer by around 34 °C. The higher values of T_{NI} shown by these series are completely in accord with the predictions made by a theoretical model developed by Luckhurst and coworkers.[7] This effect can be explained by the change in nature of the link between the flexible spacer and one of the mesogenic units giving a more linear molecular shape, Fig. 12, and this effect was similarly described by Walker *et al.*[53]

Changing the terminal linking group has a consistent effect over all six of the series reported, replacing an oxygen terminal linking group with a sulfur-linking group sees T_{NI} decrease by 39 °C from the CBO5O·Om to the CBO5O·Sm series, and by 40 °C for the CB6O·Om and CB6O·Sm series. The methylene-linked series showed intermediate values compared to the oxygen- and sulfur-linked series with the difference in T_{NI} between the CBO5O·m and CBO5O·Sm series being 17 °C and for the CB6O·m and CB6O·Sm series this decrease is 16 °C. This change in transition temperatures reflects the fact that the sulfur and oxygen linking groups show the largest difference in bond angles, with oxygen-linked dimers having the largest bond angle connecting the mesogenic unit and the alkyl chain, C–O–C, which was calculated by DFT to be 119°. This makes it the most linear of the three linking groups. The sulfur-linked dimers are the least linear, due to the C–S–C bond angle, found to be 100.5° and this is also narrower than the C–C–C bond

angle, which was calculated by DFT to be 113.5°. A linear structure is more compatible with the molecular organisation found in the nematic phase and this leads to increased values of T_{NI}. The more acute bond angle of C–S–C means that the terminal chain protrudes at more of an angle which reduces the shape anisotropy, as well as disrupting the packing efficiency of the molecules, Fig. 13.

The exception to the outlined trend is found for the dimers with $t = 2$ for which a higher value of T_{NI} is seen for both sulfur-linked series compared to the carbon-linked ones. This behaviour has been accounted for potentially in terms of chalcogen bonding with regards to the nSCB series.[19] However, single crystal studies have suggested that there were no S–S contacts in the CB6O·Sm series although this does not preclude these interactions from being present in the nematic phase.[52] Similar anomalous behaviour is observed for other mesogens with terminal alkylthio chains and in those cases were attributed to the larger dispersion force of the polarisable sulfur atom when compared to oxygen and carbon.[60] It is unclear why such a small structural change in chain length has such a large impact on the transition temperatures. This trend does appear to be very consistent over a range of compounds with a sulfur-linked terminal chain.[19,52,60–62]

The dependence of T_{NTBN} on the length of the terminal chain up to a total terminal chain length of 10 is shown in Fig. 11(b). By first considering the series with an O5O spacer, the CBO5O·Om series has the highest values of T_{NTBN} and the CBO5O·Sm series the lowest as would be expected from previous observations for the conventional nematic phase due to the bond angle of the terminal linking group. However, while
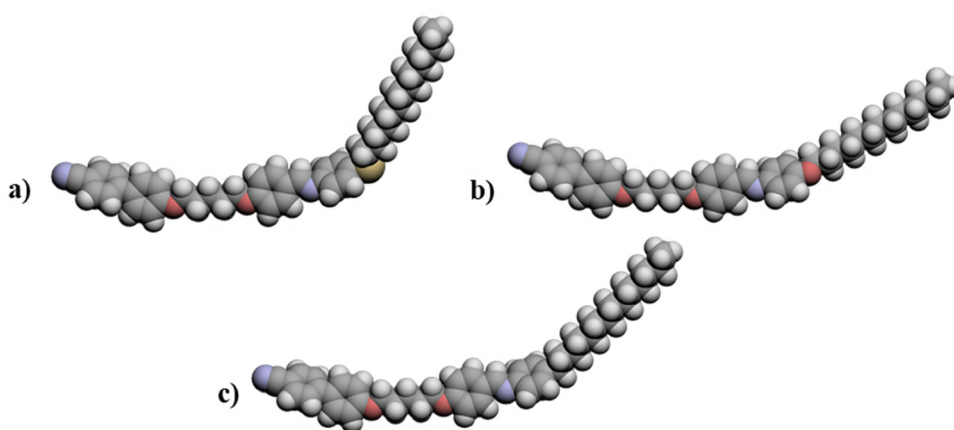

Fig. 13 A comparison of the molecular shapes of (a) CBO5O·S13; (b) CBO5O·O13 and (c) CBO5O·14.

T_{NTBN} is on average 27 °C lower for both series of sulfur-linked dimers compared to the oxygen-linked dimers, these values are only 7 °C lower than the carbon-linked dimers.

The anomalous transition temperatures which were seen for the conventional nematic phase are also seen for the N_{TB} phase when $t = 2$. CB6O·S1 has a value of T_{NTBN} only 4 °C lower than CB6O·O1 and some 14 °C higher than CB6O·2, presumably due to the same interaction being present. This effect was not observed for the CBO5O·Sm series but that is simply due to the early onset of crystallisation inhibiting the observation of the N_{TB} phase. For each corresponding pair of series, the more linear nature of the materials containing two ether linking groups (O5O spacer) might be expected to decrease the values of T_{NTBN} relative to those of the corresponding dimers with only one ether linking group (6O spacer). Indeed, this is the case for the CBO5O·Om and CB6O·Om series with values of T_{NTBN} around 9 °C higher for the latter. The transition temperatures of the CBO5O·m and CBO5O·Sm series are fairly similar in value to the CB6O·m and CB6O·Sm series, respectively, although the dimers with a 6O spacer have generally slightly higher temperatures. This might be somewhat unexpected when considering difference in T_{NTBN} seen for the oxygen-linked dimers, however, an explanation for this was reported by Walker *et al.*[53] who suggested that an enhanced specific interaction existed in the CBO5O·m series providing an additional driving force compared to the CB6O·m series.

The dependence of the onset temperature of the SmC$_{TB-SH}$ phase on the length of the terminal chain is shown in Fig. 11(c). All six of the series exhibit the SmC$_{TB-SH}$ phase and the transition temperatures tend to increase with increasing terminal chain length. This may be attributed to the elongated terminal chains allowing both the shape anisotropy to become more well-defined, as well as promoting molecular inhomogeneity between the mesogenic units and alkyl chains which stabilises the layered arrangement of the smectic phase due to microphase separation.[63] This may suggest that molecular inhomogeneity is of key importance for the formation of the SmC$_{TB-SH}$ phase much like more conventional smectic phases. Intriguingly the trends in the phase behaviour are more similar to those seen for the conventional nematic phase rather than the N_{TB} phase, although there are some key differences. The CBO5O·Om series in general has the highest upper limit for the observation of the SmC$_{TB-SH}$ phase followed by the CBO5O·m series. However, when $t = 18$ the difference between CBO5O·18, CB6O·O17 and CB6O·18 is relatively small with all the transitions being observed within a 4 °C span. The two sulfur-linked series, namely, CBO5O·Sm and CB6O·Sm, both have relatively low transition temperatures to the SmC$_{TB-SH}$ phase compared to the other series with the CB6O·Sm series having the lowest values due to the protrusion of the terminal chain as was described for T_{NI}. The trend seen when varying the nature of the terminal linking groups, from oxygen to carbon to sulfur, mirrors that discussed earlier and so the reduction in the shape anisotropy, and disruption in packing efficiency also hold here. The onset of the SmC$_{TB-SH}$ phase, the chain length at which the phase is first observed in a series, seems to vary

depending on the molecular architecture of the dimers. The three series containing a O5O spacer exhibit the phase at shorter terminal chain lengths than those with a 6O spacer and similarly the O5O spacer dimers, in general, exhibit higher transition temperatures than their 6O equivalents. The O5O dimers have a more linear shape, Fig. 12, which is more favourable for packing the molecules into layered structures as is found in smectic phases. However, this is somewhat surprising considering this means molecular bend is reduced which may seem a disadvantage for arranging the molecules also into a twist-bend heliconical structure. Presumably while molecular bend is a prerequisite driving force for the observation of the SmC$_{TB-SH}$ phase, and hence the observation in dimers with an odd-membered spacer, we also have to consider effects that promote smectic phases such as enhanced microphase separation and increased linearity as additional drivers of the phase. It appears here that increased linearity, while maintaining some bend, is actually the most favourable for the observation of the SmC$_{TB-SH}$ phase. What is key to our understanding of the transition temperatures seen for the SmC$_{TB-SH}$ phase is the interaction between these different effects, and more compounds which exhibit the phase are needed in order to fully understand exactly which of these interactions has the largest effect on the phase behaviour observed.

Conclusions

The dimers reported here provide new examples of materials exhibiting two spontaneously heliconical liquid crystal phases, the N_{TB} and SmC$_{TB-SH}$ phases. The N_{TB} phase is observed when the terminal alkyl chains are short, regardless of the nature of the linking group, whereas when the terminal alkyl chains are long there is a predisposition towards more smectic-like behaviour, including the rarely observed SmC$_{TB-SH}$ phase. The nature of the link attaching the terminal chain, either ether, thioether or methylene, also influences the stability of these LC phases with mesogens featuring ether-linked terminal chains promoting the formation of both the N_{TB} and SmC$_{TB-SH}$ phases. In addition to the effect of their terminal chains, the central spacer linking the mesogenic units plays a key role in determining the phase behaviour of the materials, particularly through its influence on the overall molecular shape, which is a key driving force in the formation of twist-bend liquid crystal phases. Comparing materials with diether-linked (O5O) spacers, to previously reported materials with hexyloxy (6O) spacers, it is interesting to note that these new materials appear to stabilize the SmC$_{TB-SH}$ phase compared to their single-ether analogues. This unexpected observation contrasts with the trends seen for the N_{TB} phase, where the more highly bent structure of dimers with a 6O spacer is considered more favourable. In the SmC$_{TB-SH}$ phase, in addition to the importance of a bent molecular shape inherent to the twist-bend phases, the formation of layered structure adds an additional complexity to the molecular design of new materials which is not fully clear. Indeed, our understanding of the structure–

property relationships and driving forces behind the formation of the SmC$_{TB-SH}$ phase are still at an embryonic stage and so it is critical that further compounds are synthesized which exhibit this exciting phase.

Conflicts of interest

There are no conflicts to declare.

Data availability

The data supporting this article have been included as part of the SI. See DOI: **https://doi.org/10.1039/d5tc02641e**

Acknowledgements

References

1 M. Cestari, S. Diez-Berart, D. A. Dunmur, A. Ferrarini, M. R. De La Fuente, D. J. B. Jackson, D. O. Lopez, G. R. Luckhurst, M. A. Perez-Jubindo, R. M. Richardson, J. Salud, B. A. Timimi and H. Zimmermann, *Phys. Rev. E: Stat., Nonlinear, Soft Matter Phys.*, 2011, **84**, 031704.

2 M. Salamończyk, R. J. Mandle, A. Makal, A. Liebman-Peláez, J. Feng, J. W. Goodby and C. Zhu, *Soft Matter*, 2018, **14**, 9760–9763.

3 D. Chen, J. H. Porada, J. B. Hooper, A. Klittnick, Y. Shen, M. R. Tuchband, E. Korbloèa, D. Bedrov, D. M. Walba, M. A. Glaser, J. E. Maclennan and N. A. Clark, *Proc. Natl. Acad. Sci. U. S. A.*, 2013, **110**, 15931–15936.

4 V. Borshch, Y. K. Kim, J. Xiang, M. Gao, A. Jákli, V. P. Panov, J. K. Vij, C. T. Imrie, M. G. Tamba, G. H. Mehl and O. D. Lavrentovich, *Nat. Commun.*, 2013, **4**, 2635.

5 W. D. Stevenson, Z. Ahmed, X. B. Zeng, C. Welch, G. Ungar and G. H. Mehl, *Phys. Chem. Chem. Phys.*, 2017, **19**, 13449–13454.

6 R. J. Mandle, C. T. Archbold, J. P. Sarju, J. L. Andrews and J. W. Goodby, *Sci. Rep.*, 2016, **6**, 36682.

7 C. Greco, G. R. Luckhurst and A. Ferrarini, *Soft Matter*, 2014, **10**, 9318–9323.

8 R. B. Meyer, in *Molecular Fluids: Les Houches Summer School in Theoretical Physics 1973*, ed. R. Balian and G. Weil, Gordon and Breach, New York, 1976, pp. 273–373.

9 I. Dozov, *Europhys. Lett.*, 2001, **56**, 247–253.

10 E. Cruickshank, M. Salamończyk, D. Pociecha, G. J. Strachan, J. M. D. Storey, C. Wang, J. Feng, C. Zhu, E. Gorecka and C. T. Imrie, *Liq. Cryst.*, 2019, **46**, 1595–1609.

11 Y. Arakawa, T. Shiba and K. Igawa, *Liq. Cryst.*, 2024, **51**, 1506–1522.

12 R. Walker, M. Majewska, D. Pociecha, A. Makal, J. M. Storey, E. Gorecka and C. T. Imrie, *ChemPhysChem*, 2020, **22**, 461–470.

13 P. A. Henderson and C. T. Imrie, *Liq. Cryst.*, 2011, **38**, 1407–1414.

14 Z. Lu, P. A. Henderson, B. J. A. Paterson and C. T. Imrie, *Liq. Cryst.*, 2014, **41**, 471–483.

15 C. J. Gibb, M. M. Majewska, G. J. Strachan, D. Pociecha, J. M. D. Storey, E. Gorecka and C. T. Imrie, *Phys. Chem. Chem. Phys.*, 2025, **27**, 6104–6110.

16 E. Cruickshank, G. J. Strachan, A. Pearson, D. Pociecha, E. Gorecka, J. M. D. Storey and C. T. Imrie, *Phys. Chem. Chem. Phys.*, 2025, **27**, 6111–6121.

17 R. J. Mandle, E. J. Davis, C. T. Archbold, C. C. A. Voll, J. L. Andrews, S. J. Cowling and J. W. Goodby, *Chem. – Eur. J.*, 2015, **21**, 8158–8167.

18 E. Forsyth, D. A. Paterson, E. Cruickshank, G. J. Strachan, E. Gorecka, R. Walker, J. M. D. Storey and C. T. Imrie, *J. Mol. Liq.*, 2020, **320**, 114391.

19 E. Cruickshank, G. J. Strachan, J. M. D. Storey and C. T. Imrie, *J. Mol. Liq.*, 2021, **346**, 117094.

20 D. A. Paterson, J. P. Abberley, W. T. A. Harrison, J. M. D. Storey and C. T. Imrie, *Liq. Cryst.*, 2017, **44**, 127–146.

21 Y. Arakawa, K. Komatsu, Y. Ishida and H. Tsuji, *Liq. Cryst.*, 2021, **48**, 641–652.

22 Y. Arakawa, K. Komatsu, T. Shiba and H. Tsuji, *Mater. Adv.*, 2021, **2**, 1760–1773.

23 D. A. Paterson, R. Walker, J. M. D. Storey and C. T. Imrie, *Liq. Cryst.*, 2023, **50**, 725–736.

24 Y. Arakawa, K. Komatsu, Y. Ishida, T. Shiba and H. Tsuji, *Materials*, 2022, **15**, 1709.

25 M. R. Tuchband, D. A. Paterson, M. Salamończyk, V. A. Norman, A. N. Scarbrough, E. Forsyth, E. Garcia, C. Wang, J. M. D. Storey, D. M. Walba, S. Sprunt, A. Jákli, C. Zhu, C. T. Imrie and N. A. Clark, *Proc. Natl. Acad. Sci. U. S. A.*, 2019, **116**, 10698–10704.

26 Y. Arakawa, K. Komatsu, S. Inui and H. Tsuji, *J. Mol. Struct.*, 2020, **1199**, 126913.

27 G. J. Strachan, M. M. Majewska, D. Pociecha, E. Gorecka, J. M. D. Storey and C. T. Imrie, *Liq. Cryst.*, 2024, **51**, 2059–2068.

28 R. J. Mandle and J. W. Goodby, *ChemPhysChem*, 2016, **17**, 967–970.

29 M. M. Majewska, E. Forsyth, D. Pociecha, C. Wang, J. M. D. Storey, C. T. Imrie and E. Gorecka, *Chem. Commun.*, 2022, **58**, 5285–5288.

30 F. P. Simpson, R. J. Mandle, J. N. Moore and J. W. Goodby, *J. Mater. Chem. C*, 2017, **5**, 5102–5110.

31 R. J. Mandle and J. W. Goodby, *Angew. Chem., Int. Ed.*, 2018, **57**, 7096–7100.

32 R. J. Mandle, *Chem. Rec.*, 2018, **18**, 1341–1349.

33 M. G. Tamba, U. Baumeister, G. Pelzl and W. Weissflog, *Ferroelectrics*, 2014, **468**, 52–76.

34 S. P. Sreenilayam, V. P. Panov, J. K. Vij and G. Shanker, *Liq. Cryst.*, 2017, **44**, 244–253.

35 S. M. Jansze, A. Martínez-Felipe, J. M. D. Storey, A. T. M. Marcelis and C. T. Imrie, *Angew. Chem., Int. Ed.*, 2015, **127**, 653–656.

36 R. Walker, D. Pociecha, A. Martinez-Felipe, J. M. D. Storey, E. Gorecka and C. T. Imrie, *Crystals*, 2020, **10**, 175.

37 D. A. Paterson, C. A. Crawford, D. Pociecha, R. Walker, J. M. D. Storey, E. Gorecka and C. T. Imrie, *Liq. Cryst.*, 2018, **45**, 2341–2351.

38 R. Walker, D. Pociecha, C. A. Crawford, J. M. D. Storey, E. Gorecka and C. T. Imrie, *J. Mol. Liq.*, 2020, **303**, 112630.

39 E. Gorecka, N. Vaupotič, A. Zep, D. Pociecha, J. Yoshioka, J. Yamamoto and H. Takezoe, *Angew. Chem., Int. Ed.*, 2015, **54**, 10155–10159.

40 R. Walker, D. Pociecha, J. M. D. Storey, E. Gorecka and C. T. Imrie, *Chem. – Eur. J.*, 2019, **25**, 13329–13335.

41 R. Walker, D. Pociecha, M. Salamonczyk, J. M. D. Storey, E. Gorecka and C. T. Imrie, *ChemPhysChem*, 2023, **24**, e202200807.

42 A. Ožegović, A. Knežević, J. Novak, S. Šegota, P. Davidson and A. Lesac, *ChemPhysChem*, 2024, **25**, e202400065.

43 R. Walker, D. Pociecha, M. Salamończyk, J. M. D. Storey, E. Gorecka and C. T. Imrie, *Mater. Adv.*, 2020, **1**, 1622–1630.

44 N. Tufaha, C. J. Gibb, J. M. D. Storey and C. T. Imrie, *Liq. Cryst.*, 2023, **50**, 1362–1374.

45 J. P. Abberley, R. Killah, R. Walker, J. M. D. Storey, C. T. Imrie, M. Salamończyk, C. Zhu, E. Gorecka and D. Pociecha, *Nat. Commun.*, 2018, **9**, 228.

46 M. Salamończyk, N. Vaupotič, D. Pociecha, R. Walker, J. M. D. Storey, C. T. Imrie, C. Wang, C. Zhu and E. Gorecka, *Nat. Commun.*, 2019, **10**, 1922.

47 C. J. Gibb, M. Majewska, D. Pociecha, J. M. D. Storey, E. Gorecka and C. T. Imrie, *ChemPhysChem*, 2024, **25**, e202300848.

48 D. Pociecha, N. Vaupotič, M. Majewska, E. Cruickshank, R. Walker, J. M. D. Storey, C. T. Imrie, C. Wang and E. Gorecka, *Adv. Mater.*, 2021, **33**, 2103288.

49 A. F. Alshammari, D. Pociecha, R. Walker, J. M. D. Storey, E. Gorecka and C. T. Imrie, *Soft Matter*, 2022, **18**, 4679–4688.

50 C. T. Imrie, R. Walker, J. M. D. Storey, E. Gorecka and D. Pociecha, *Crystals*, 2022, **12**, 1245.

51 A. F. Alshammari, A. Zattarin, A. Pearson, E. Cruickshank, M. Majewska, D. Pociecha, J. M. D. Storey, E. Gorecka, C. T. Imrie and R. Walker, *Liq. Cryst.*, 2024, **51**, 2300–2312.

52 E. Cruickshank, K. Anderson, J. M. D. Storey, C. T. Imrie, E. Gorecka, D. Pociecha, A. Makal and M. M. Majewska, *J. Mol. Liq.*, 2022, **346**, 118180.

53 R. Walker, D. Pociecha, G. J. Strachan, J. M. D. Storey, E. Gorecka and C. T. Imrie, *Soft Matter*, 2019, **15**, 3188–3197.

54 E. Cruickshank, R. Walker, G. J. Strachan, C. H. F. Goode, M. M. Majewska, D. Pociecha, E. Gorecka, J. M. D. Storey and C. T. Imrie, *J. Mol. Liq.*, 2023, **391**, 123226.

55 G. S. Attard, R. W. Date, C. T. Imrie, G. R. Luckhurst, S. J. Roskilly, J. M. Seddon and L. Taylor, *Liq. Cryst.*, 1994, **16**, 529–581.

56 M. J. Frisch, G. W. Trucks, H. B. Schlegel, G. E. Scuseria, M. A. Robb, J. R. Cheeseman, G. Scalmani, V. Barone, B. Mennucci, G. A. Petersson, H. Nakatsuji, M. Caricato, X. Li, H. P. Hratchian, A. F. Izmaylov, J. Bloino, G. Zheng, J. L. Sonnenberg, M. Hada, M. Ehara, K. Toyota, R. Fukuda, J. Hasegawa, M. Ishida, T. Nakajima, Y. Honda, O. Kitao, H. Nakai, T. Vreven, J. A. Montgomery, J. E. Peralta, F. Ogliaro, M. Bearpark, J. J. Heyd, E. Brothers, K. N. Kudin, V. N. Staroverov, R. Kobayashi, J. Normand, K. Raghavachari, A. Rendell, J. C. Burant, S. S. Iyengar, J. Tomasi, M. Cossi, N. Rega, J. M. Millam, M. Klene, J. E. Knox, J. B. Cross, V. Bakken, C. Adamo, J. Jaramillo, R. Gomperts, R. E. Stratmann, O. Yazyev, A. J. Austin, R. Cammi, C. Pomelli, J. W. Ochterski, R. L. Martin, K. Morokuma, V. G. Zakrzewski, G. A. Voth, P. Salvador, J. J. Dannenberg, S. Dapprich, A. D. Daniels, O. Farkas, J. B. Foresman, J. V. Ortiz, J. Cioslowski and D. J. Fox, Gaussian, Inc., Wallingford CT, 2010.

57 M. Tarini, P. Cignoni and C. Montani, *IEEE Trans. Vis. Comput. Graph.*, 2006, **12**, 1237–1244.

58 R. L. Humphries, P. G. James and G. R. Luckhurst, *Symp. Faraday Soc.*, 1971, **5**, 107–118.

59 C. T. Imrie and L. Taylor, *Liq. Cryst.*, 1989, **6**, 1–10.

60 Y. Arakawa, Y. Ishida, T. Shiba, K. Igawa, S. Sasaki and H. Tsuji, *CrystEngComm*, 2022, **24**, 1877–1890.

61 E. Cruickshank, G. J. Strachan, M. M. Majewska, D. Pociecha, E. Górecka, J. M. D. Storey and C. T. Imrie, *New J. Chem.*, 2023, **47**, 7356–7368.

62 Y. Arakawa, Y. Ishida, Y. Sasaki, S. Sasaki, M. Tokita and H. Tsuji, *Mater. Adv.*, 2022, **3**, 3218–3228.

63 R. W. Date, C. T. Imrie, G. R. Luckhurst and J. M. Seddon, *Liq. Cryst.*, 1992, **12**, 203–238.